

## A NONLINEAR THREE-DIMENSIONAL ANALYSIS OF REINFORCED CONCRETE BASED ON A BOUNDING SURFACE MODEL

T. PAGNONI,† J. SLATER,‡ R. AMEUR-MOUSSA§ and O. BUYUKOZTURK¶  
 Department of Civil Engineering, Massachusetts Institute of Technology, Cambridge,  
 MA 02139, U.S.A.

(Received 28 March 1991)

**Abstract**—The present work addresses the problem of the formulation of an accurate yet efficient finite element procedure for the nonlinear analysis of general three-dimensional reinforced concrete structures. The main objectives of the research are: (1) the extension and recalibration of an existing bounding surface model for the behavior of concrete in cyclic compression; (2) the development of a complete constitutive relation for reinforced concrete by combining the bounding surface model with numerical procedures for the modeling of crack propagation, tension stiffening and steel reinforcement interaction effects; and (3) the implementation of the constitutive model in a three-dimensional isoparametric eight-node element. The accuracy of the proposed model is successfully demonstrated by detailed analyses of a deep beam and a prestressed concrete reactor vessel.

### NOTATION

$A_i, A_u, \lambda$	model parameters	$K, dK, K_{max}$	damage parameter, its increment, and its maximum value
$C_{ijkl}$	compliance tensor	$K_R, K_u$	associated $K$ value at beginning of recent loading and unloading process, respectively
$D, D', D_i$	rigidity matrix of concrete, at time, $t$ , and at iteration $i$	$K_t$	tangent bulk modulus
$\hat{D}, d\hat{D}$	normalized distance, and its increment	$l_c$	characteristic length for concrete cracking
$\hat{\epsilon}_{ij}, d\hat{\epsilon}_{ij}$	normalized deviatoric strain tensor, and its increment	$R$	distance of bounding surface from hydroaxis along $S_y$ direction
$\hat{\epsilon}_{ij}^e, d\hat{\epsilon}_{ij}^e$	normalized deviatoric strain due to elastic response, and its increment	$r$	distance from projection of current stress point on deviatoric plane to the hydroaxis
$\hat{\epsilon}_{ij}^p, d\hat{\epsilon}_{ij}^p$	normalized deviatoric strain due to plastic response, and its increment	$r_i$	internal forces vector at iteration $i$
$F$	bounding surface	$\hat{S}_{ij}, d\hat{S}_{ij}$	normalized deviatoric stress tensor, and its increment
$F_1$	normalization factor	$\Delta u_i$	displacement increment vector at iteration $i$
$f'_c$	concrete strength in uniaxial compression	$\alpha$	stiffening parameter
$f'_t$	concrete strength in uniaxial tension	$\beta$	shear compaction-dilatancy factor
$G, G^*$	shear modulus, and shear modulus of cracked concrete	$\beta_1$	shear compaction factor
$G_f$	fracture energy of concrete	$\beta_2$	shear dilatancy factor
$H^p$	generalized plastic shear modulus	$\epsilon, \epsilon_0$	uniaxial strain, its value associated to $f'_t$
$I_1, dI_1, I_{1,max}$	first normalized stress invariant, its increment, and its maximum value	$\epsilon_i, \Delta\epsilon_i, \epsilon'$	strain vector at iteration $i$ , its increment, and at time $t$
$J_2, J_3$	second and third normalized deviatoric stress invariants	$\epsilon_n^*, \epsilon_{n,max}^*$	fictitious tensile strain normal to a crack, and its maximum value
		$\hat{\epsilon}_{ij}, d\hat{\epsilon}_{ij}$	normalized strain tensor, and its increment
		$\epsilon_p$	associated axial strain to $f'_c$ in uniaxial loading
		$\hat{\gamma}_6^p, d\hat{\gamma}_6^p$	normalized plastic octahedral shear strain and its increment
		$\theta$	angle between projections of position vector of principal stress and that of any tensile semiaxis on deviatoric plane
		$\hat{\tau}_0, d\hat{\tau}_0$	normalized octahedral shear stress, and its increment
		$\sigma$	uniaxial stress
		$\sigma_i, \Delta\sigma_i, \sigma'$	stress vector at iteration $i$ , its increment, and at time $t$
		$\hat{\sigma}_{ij}, d\hat{\sigma}_{ij}$	stress tensor, its increment and its principal values
		$\hat{\sigma}_I, \hat{\sigma}_{II}, \hat{\sigma}_{III}$	

† Department of Civil Engineering, MIT, Cambridge, MA 02139, U.S.A.

‡ Stone & Webster Advanced Systems Development, Services, P.O. Box 2325, Boston, MA 02109, U.S.A.; formerly with Department of Civil Engineering, MIT, Cambridge, MA 02139, U.S.A.

§ Souza & True, Watertown, MA 02172, U.S.A.; formerly with Department of Civil Engineering, MIT, Cambridge, MA 02139, U.S.A.

¶ Department of Civil Engineering, MIT, Cambridge, MA 02139, U.S.A. To whom correspondence should be addressed.

## INTRODUCTION

The need for an accurate prediction of the response of complex reinforced concrete structures has stimulated conspicuous research activity in the field of computational analysis of reinforced concrete structures during the last 20 years. Advances in the areas of finite elements, concrete constitutive modeling and nonlinear solution techniques have made sophisticated analysis of this complex composite material possible. Nevertheless, several aspects of the current analysis methods are still unsatisfactory. A major problem with the applicability of state-of-the-art finite element analysis of reinforced concrete structures to realistic problems is that sufficient accuracy is often accompanied by excessive computational costs. Undoubtedly, many important aspects of reinforced concrete behavior make its analysis rather complicated. Among these are: the nonlinear multi-axial stress-strain response; the shear compaction-dilatancy phenomenon; the strain softening behavior and the stiffness degradation in cyclic loading. In addition, the formation and propagation of diffuse microcracks which coalesce into localized fracture zones is often a dominating component of the nonlinear structural response. Furthermore, the composite nature of the material introduces additional difficulties in modeling the interactions between reinforcement and concrete. Each of the aspects of the material behavior mentioned have been studied extensively and several alternative approaches have been suggested, but no general agreement has been reached.

There is a critical need for the development of a finite element approach based on a constitutive model consistent with these aspects of the phenomenological behavior of concrete. This paper represents our effort in answering this need by: (1) extending and recalibrating an existing bounding surface model [1] for concrete behavior in cyclic compression; (2) developing a complete constitutive relation for reinforced concrete by combining the bounding surface model with numerical procedures for the modeling of crack propagation, tension stiffening and steel reinforcement interaction effect; (3) implementing the constitutive model in a three-dimensional isoparametric eight-node brick which has been successfully tested in several example problems.

The remainder of this paper is divided in four parts. In the following section, the extensions and recalibrations of the bounding surface model are presented. Next, the adopted models for post-cracking behavior are examined. Thereafter, the nonlinear solution methods used in the analysis of concrete structures are reviewed and the procedures adopted in this work are discussed. Finally, the results of finite element analysis of a deep beam and a prestressed concrete reactor vessel are presented. They compare favorably with the experimental results.

## MODEL OF CONCRETE BEHAVIOR IN COMPRESSION

Numerous models for the behavior of concrete in compression have been proposed during the last 15 years. A comprehensive review of these models may be found in [2-5]. Although many of these models can describe the behavior of concrete in monotonic loadings, only a few of them are capable of describing the complex multi-axial cyclic behavior. Among these models, considerations of numerical efficiency led us to focus attention on a previously proposed bounding surface model [1]. Such a model accurately predicts the nonlinear stress-strain response, stiffness degradation during load cycles, the shear compaction and dilatancy and the strain softening in uniaxial loading. This model, however, does not provide a satisfactory prediction near and beyond ultimate strength for triaxial states of stress [2]. A modified version of the model which extends its range of applicability is developed as part of this work. The most significant improvement introduced to the model are:

- (a) the recalibration of the damage formulation using a large amount of experimental data,
- (b) the formulation of a new bounding surface equation based on a large set of experimental data including recently produced experiment results from cyclic loading with triaxial compression [6],
- (c) the introduction of hydrostatic pressure sensitivity in the post-failure zone to allow more realistic modeling of the strain softening behavior.

In addition, the model has been made applicable to a wide range of concretes by expressing the material constants as functions of the uniaxial compressive strength of concrete and the corresponding peak strain.

It should be noted that recent studies, e.g. [7], have shown that the strain softening behavior of concrete is not a material property, but rather a structural property, in the sense that the geometry of the surrounding structure directly influences the softening behavior. As a result, the stress-strain relationship should reflect the effect of finite element size. However, due to the lack of experimental data on the post-failure behavior of concrete, the development of a consistent three-dimensional model in the post-peak phase is premature [4]. A continuum approach is, therefore, adopted in the present model, i.e., the incremental compliance relationships are assumed to hold in both the pre-failure and post-failure ranges.

In the following sections, the bounding surface concept is briefly reviewed, and the essential aspects of the proposed model are described (details can be found in [1, 2]). Note that in the following formulation, stresses and strains are normalized with respect to the uniaxial compressive strength and the

associated peak strain, respectively. Normalized quantities are indicated with a circumflex ( $\hat{\ }^{\circ}$ ).

*The bounding surface concept*

The bounding surface is defined as the innermost locus of all achievable points in stress space that also encloses the current state of stress. In contrast to the classical plasticity theory, where loading and unloading criteria are defined in terms of yield and loading surfaces, bounding surface models do not postulate *a priori* the existence of such surfaces. The bounding surface concept is linked with the idea of irreversible damage. This concept expresses at the macroscopic level a bounding material state resulting from microscopic defects. Material damage (micro-cracking, crushing) is accounted for by contracting the bounding surface in stress space as damage accumulates.

In order to obtain a scalar measure of damage, a mapping rule is required. Following [1], a radial mapping in the deviatoric plane containing the stress point is used to associate an 'image' stress point on the bounding surface with any given stress point within the surface. The rate of plastic deformation is expressed as a function of the distance between the current stress point and its 'image' on the bounding surface. Figure 1 illustrates the previous concepts.

*Damage representation*

For deviatoric loading and unloading, it is proposed that the damage be expressed as a function of the stress state using the normalized distance  $D$  from the stress point to the hydrostatic axis in the deviatoric plane. This normalized distance may be expressed in terms of  $\hat{J}_2$ , the second invariant of the normalized deviatoric stress. In the post-failure range, however, the stress point lies continuously on the bounding surface, because the bounding surface shrinks with increasing strain. This results in a constant post-failure value of  $D = 1$ . Hence, a strain

measure based on the plastic octahedral shear strain  $\hat{\gamma}_0^p$  is chosen to represent damage in the post-failure range.  $\hat{\gamma}_0^p$  is a good measure of the overall plastic straining in the deviatoric plane. Using these ideas, the following incremental formulations were proposed in [1]:

1. For deviatoric loading and unloading

$$dK = \frac{R dD}{H^p F_1(\hat{I}_1, \theta)} \quad (1)$$

2. In the post-failure range

$$dK = \frac{d\hat{\gamma}_0^p}{F_1(\hat{I}_1, \theta)} \quad (2)$$

where  $\hat{I}_1$  is the first invariant of the normalized stress tensor, and  $\theta$  is the angle between the projections of the position vector of the principal stress and that of any tensile semiaxis on the deviatoric plane. The total damage  $K$  is obtained by integrating the rate of damage  $dK$  along the stress path.  $H^p$  is the plastic shear modulus. The function  $F_1(\hat{I}_1, \theta)$  accounts for the hydrostatic pressure and stress path dependency of the behavior of concrete on the deviatoric plane. This function is chosen to normalize  $K$  so that it reaches the value of 1.0 at failure under monotonic loading. Using test data from monotonic [6, 8-10] and cyclic [6, 11, 12] loadings, with cycle ranges of 0-85%, 30-95%, and 40-95% of the uniaxial compressive strength in both confined and unconfined loading, the following regression forms are proposed:

1. For deviatoric loading

$$F_1(\hat{I}_1, \theta) = \frac{0.248\hat{I}_1^2 + 0.182\hat{I}_1}{G(\cos 3\theta)}, \quad \hat{I}_1 \leq 2 \quad (3)$$

$$F_1(\hat{I}_1, \theta) = \frac{1.867\hat{I}_1 - 2379}{G(\cos 3\theta)}, \quad \hat{I}_1 > 2. \quad (4)$$

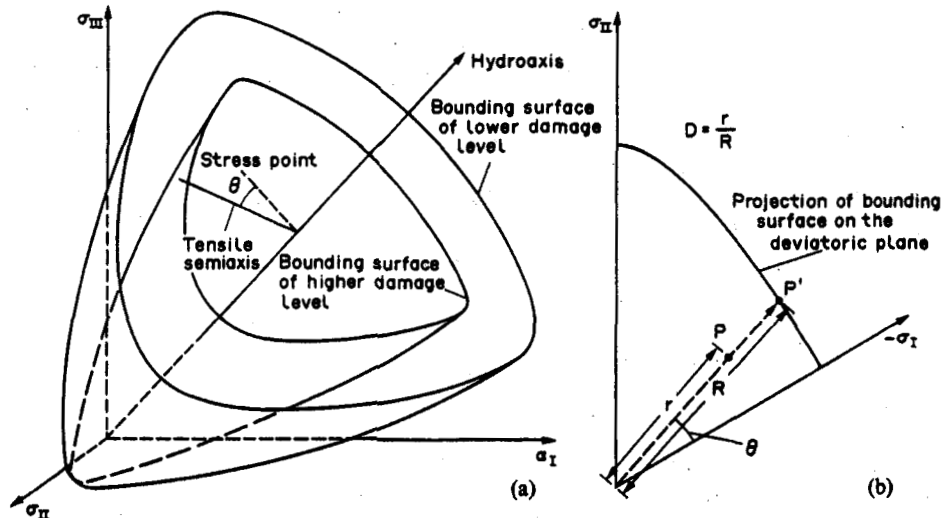


Fig. 1. The bounding surface model: (a) bounding surface, (b) radial mapping (from [1]).

## 2. For deviatoric unloading

$$F_1(\hat{I}_1, \theta) = 1.4 \left[ 0.85 - \frac{\hat{I}_1 + 0.3}{\hat{I}_{1,\max} + 0.3} \right] \frac{F_{1,\max}}{G(\cos 3\theta)} \quad (5)$$

$\hat{I}_{1,\max}$  and  $F_{1,\max}$  are respectively the maximum  $\hat{I}_1$  and  $F_1$  before the most recent unloading. The function  $G(\cos 3\theta)$  is obtained from the biaxial data in [10, 13–15] and the triaxial data in [7, 14]. The following expression is found to be adequate

$$G(\cos 3\theta) = 0.25(\cos 3\theta + 5). \quad (6)$$

### Bounding surface

An important feature of the present model is the revised bounding surface equation. The bounding surface is defined as the innermost surface in stress space that encloses all the possible stress points, for a given damage level. This surface is given as a function of the stress state and  $K_{\max}$ , the maximum value of damage ever experienced by the material

$$F(\hat{\sigma}_{ij}, K_{\max}) = 0. \quad (7)$$

Using the available experimental data [6–8, 10, 13–15], the coefficients of the bounding surface equation proposed in [1] are recalibrated by regression analysis and the following expression for the failure surface is obtained

$$F(\hat{\sigma}_{ij}, K_{\max}) = \frac{0.25\hat{J}_2 + 3.10\sqrt{\hat{J}_2}}{4\hat{I}_1 + 3.48} (\cos 3\theta + 5) - \frac{40}{39 \times K_{\max}^2} \quad (8)$$

### Incremental stress–strain law

As in incremental plasticity, the strain increment is decomposed into its elastic and plastic components, and the following incremental compliance law is derived [1, 2]

$$d\hat{\epsilon}_{ij} = C_{ijkl} d\hat{\sigma}_{kl} \quad (9)$$

$$C_{ijkl} = \frac{1}{2G} \delta_{ik} \delta_{jl} + \frac{1}{3H^p \hat{\epsilon}_0} \left( \frac{\hat{S}_{ij}}{\hat{\epsilon}_0} + \delta_{ij} \frac{\beta}{3} \right) \hat{S}_{kl} + \left( \frac{1}{9K_t} \frac{1}{6G} \right) \delta_{ij} \delta_{kl}. \quad (10)$$

In displacement-based finite element analysis, the compliance matrix obtained from the above expression is inverted to obtain the material rigidity matrix. It is worth noting that this matrix is not symmetric due to the coupling between deviatoric stresses and volumetric strains. Following (9), in the present finite element implementation, only the symmetric part of the stiffness matrix is considered for stiffness assemblage.

All the material parameters used in this constitutive model are determined through regression analysis using the available experimental results for concrete. Their analytical expressions are given in the Appendix. It should be noted that the data provided in [14] have been used to develop an expression for the plastic shear modulus in the post-failure range which accounts for the hydrostatic pressure dependent behavior of concrete. As a result, the brittle behavior at low confining pressure (steep softening branch), and the rather ductile behavior at high confining pressure (almost perfectly plastic), are both predicted accurately.

### Comparison with experimental data

The proposed model accurately predicts the monotonic behavior of concrete. As an example, Fig. 2 illustrates the comparison with the test results provided by Kotsovos and Newman [9]; the overall response is good, although a –40% underestimation of the radial strain at failure is predicted. The model prediction of the cyclic behavior is satisfactory for uniaxial and biaxial loading. In the cyclic loading between two values of compressive axial stress examined by Soon [6], the principal strain is satisfactorily predicted, whereas the radial tensile strain is underestimated by –25% (cf. Fig. 3a).

The biaxial cyclic behavior of concrete is also found to be predicted accurately. A displacement controlled plane strain biaxial test to the failure envelope by Buyukozturk *et al.* [11, 16] (which results in nonproportional loading) is shown in Fig. 3(b). However, the unloading path is not predicted well, and hence, the energy dissipation is substantially

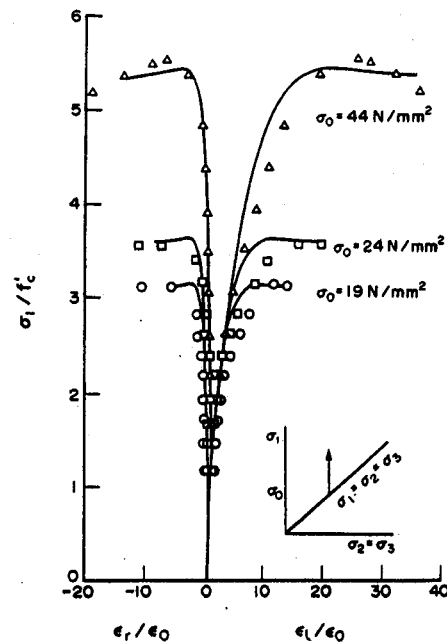


Fig. 2. Model prediction in triaxial monotonic loading: test data from [9].

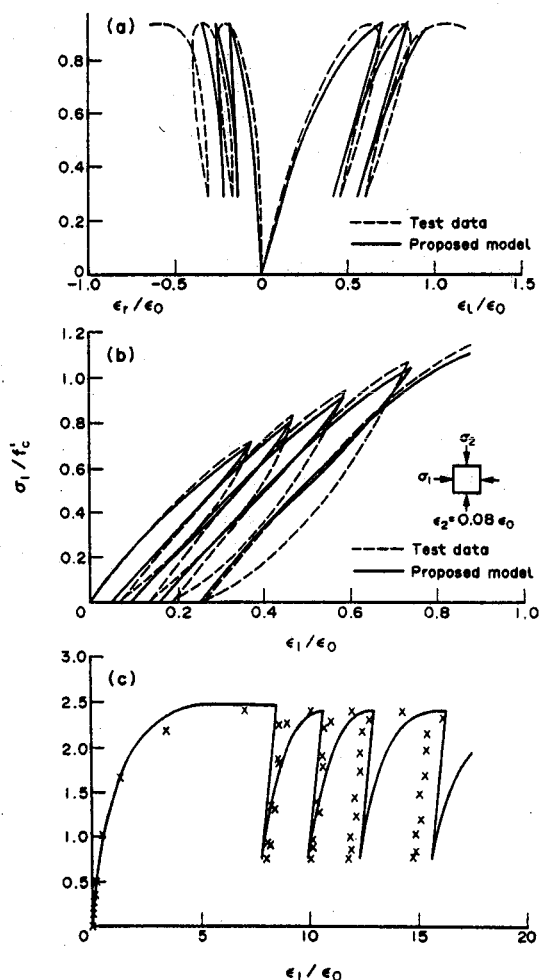


Fig. 3. Model prediction in cyclic loading: (a) uniaxial test data from [6]; (b) biaxial test data from [11, 16]; (c) triaxial test data from [6].

underestimated. The overall prediction is satisfactory. The model correctly captures the loading path, peak stress and permanent deformations.

It is only recently that triaxial cyclic data for concrete have become available [6, 7]. In trying to predict the triaxial cyclic behavior of concrete with the proposed model [2], two difficulties are generally encountered: (1) the energy dissipation during load cycles is negative, and (2) the large hysteresis loop corresponding to the first load cycle is not accurately described, i.e., the plastic strain is underestimated. However, if the principal compressive strain before the first load reversal is prescribed, a satisfactory prediction is achieved for the triaxial cyclic loading of concrete between two values of the principal stress. The test results obtained by Soon [6], in which the radial confining stress equaled 1200 psi and the principal stress was cycled between 30 and 95% of the average monotonic strength, are reasonably well predicted (cf. Fig. 3c). Based on these results, relatively little refinement to the present model is needed to obtain a realistic model of the behavior of concrete

under triaxial cyclic compressive stresses. An extension of the model is feasible and should be the subject of further research.

#### MODEL OF POST-CRACKING BEHAVIOR

Concrete cracking represents one of the most important causes of nonlinearity in the material response. Hence, a realistic prediction of ultimate loads and failure modes cannot be achieved without careful modeling of the complex phenomena which accompany the formation and propagation of cracking in the structure. Some phenomena, such as the evolution of post-crack material parameters, aggregate interlocking, the interaction between concrete and reinforcement and multiple cracks opening and closing, still represent a research challenge. In the present study we propose an integrated model of post-cracking behavior incorporating those aspects which we regard as the salient ingredients of a realistic description of the overall behavior of reinforced concrete structures. The main characteristics of the model are: (1) a smeared representation of cracks in which objectivity is preserved, and (2) the modeling of concrete-reinforcement interaction by a variable shear modulus and tension stiffening.

#### Crack modeling

In FE (finite element) analysis of reinforced concrete, two types of crack models have been proposed. A discrete crack approach with predefined crack locations [17] and with automatic crack pattern generation [18] have been investigated. The complex task of redefining the structural topology at each crack formation has stimulated the development of the so-called 'smeared crack' approach [19]. In the smeared crack approach, automatic generation of cracks with arbitrary directions is achieved with small computational effort. Recent studies [20–22] have, in part, overcome the limitations of the original formulation, which did not deal with objectivity and localized fracture. The specific version of the smeared crack model adopted for this study is outlined in the following paragraph.

The material is assumed to behave linearly under tensile stresses. When a maximum strength criterion is met, the material is assumed to crack in a plane orthogonal to the maximum tensile stress. This is represented by a modification of the material moduli in the principal stress frame and a gradual release of tension stress in the direction orthogonal to the crack. The Young's modulus in the direction orthogonal to the crack is set to zero, and the shear modulus relative to the crack plane is gradually decreased. This is described in greater detail later, in the section 'Shear transfer'. The method used for stress release can have considerable influence on the global response. No general method performs satisfactorily in all situations [23]. Two alternative procedures—tension

softening and tension stiffening—are provided in this model in order to cope with most cases.

#### *Tension softening*

The formation and propagation of micro-cracks are largely responsible for the behavior of concrete in tension. Micro-cracks, which are initially distributed on a wide area, tend to localize in a fracture zone and originate a macrocrack as the stress approaches the tensile strength. Tension softening is a term used to characterize the evolution of the stress state within a fracture zone.

The tension softening model illustrated in [22] has the important property of objectivity in the sense that the predicted crack pattern is relatively mesh independent. The simple formulation makes its implementation computationally efficient. In this model, which has been adopted in our work, the tensile stress after cracking decreases exponentially according to the following equation

$$\sigma = f'_t \exp\left(-\frac{(\epsilon - \epsilon_0)f'_t l_c}{G_f}\right), \quad (11)$$

where  $f'_t$  is the tensile strength of concrete;  $\epsilon$  is the tensile strain in the direction orthogonal to the crack plane;  $\epsilon_0$  is  $f'_t/E_0$ ,  $G_f$  is the fracture energy of concrete, regarded as a material property, and  $l_c$  is a characteristic length, here assumed equal to the cube root of the volume associated with the integration point where the crack occurred.

The characteristic length  $l_c$  establishes a dependence between the element size and the softening portion of the stress strain relation of the material, making the objectivity of the element possible.

#### *Tension stiffening*

The concrete between consecutive cracks along the reinforcements can still transmit tension stresses, contributing thereby to the stiffness of the structure. This is the well known tension stiffening effect. In the context of the finite element analysis of reinforced concrete, two methods have been suggested to account for this important effect: either an increase of the steel stiffness [24]; or a gradual decrease of the tensile stress in the cracked concrete as opposed to an abrupt stress release [25, 26]. Comparative studies [27, 28] have shown the considerable influence of the form of the descending branch on the global structural response. In this model we adopt a linear softening function represented in Fig. 4.

The stiffening parameter  $\alpha$  determines the importance of the effect. The strain corresponding to a complete stress release as  $\alpha\epsilon_0$ . No general agreement on the choice for the value for  $\alpha$  has been reached. Higher values of  $\alpha$  seem more appropriate for flexural type cracking, with an upper bound for  $\alpha\epsilon_0$  being the yield strain of the reinforcement.

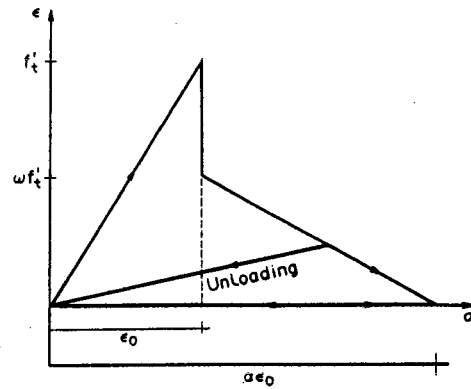


Fig. 4. Tension stiffening model.

#### *Shear transfer*

The dowel action of the reinforcing steel and aggregate interlocking contribute to the considerable residual shear stiffness to the cracked concrete, and cannot be neglected in the analysis. Several studies [25, 29, 30] modeled this phenomenon by retaining a reduced, but non-zero, constant shear modulus for the cracked concrete. A more accurate procedure [31], adopted in this study, assumes that the cracked shear modulus,  $G^*$ , decreases linearly with  $\epsilon_n^*$ , the fictitious tensile strain normal to the crack.  $G^*$  is set to zero for  $\epsilon_n^* \geq \epsilon_{n,max}^*$ . Some numerical experiments [30] suggest a range of 0.001–0.004 for  $\epsilon_{n,max}^*$ , with lower values for shear type fractures and higher values for flexural fractures.

### NONLINEAR SOLUTION METHODS

The selection of the appropriate numerical procedure for the solution of the nonlinear problem in reinforced concrete FE analyses is of utmost importance. It has been found that in a highly nonlinear material such as concrete—which exhibits peculiar characteristics like cracking and strain softening—an inappropriate algorithm selection may prevent the convergence of the solution or produce a grossly mistaken one. On the other hand, one of the major obstacles to the diffusion of the FE analysis of concrete is the tremendous demand in computational resources involved in the solution of realistic problems. Consequently, the efficiency of the adopted numerical procedure is as important as the accuracy of the constitutive model [32].

In displacement-based nonlinear FE analysis, where the basic unknowns are the displacements, three aspects of the solution are common to the various methods: the evaluation of the displacement increments, the computation of stresses given strains, and finally the definition of a convergence criterion.

For the displacements evaluation a modified Newton–Raphson solution scheme has been adopted. It has been our experience that with this algorithm the load step size may have a substantial effect on the solution. In fact, with large load increments, the

initial trial displacement field may prematurely crack a large portion of the model. In reality, a more accurate stress redistribution would have relieved those high stresses and strains in the structure. This fact confirms that the numerical solution of reinforced concrete FE problems still requires an experienced analyst for the selection of the appropriate parameters for the problem under examination.

At each integration point (typically eight per element for the linear brick element) and for each iteration within each load step, the stresses corresponding to the current strain field have to be evaluated exactly in order to determine the out-of-balance forces. When the constitutive model is defined, as in this case, by an incremental formulation, these stresses are obtained by the following integration

$$\Delta\sigma_i = \int_{\epsilon_i'}^{\epsilon_i'+\Delta\epsilon_i} \mathbf{D} d\epsilon_i \quad (12)$$

The importance of this integration is twofold: first, an inaccurate stress recovery will make the equilibrium iteration useless; second, the large number of times that this integration has to be performed—which may well be in the order of  $10^6$ – $10^7$ , requires particular attention to the efficiency of its numerical implementation.

The following 'midstep' approximation, which uses an average value of  $\mathbf{D}$ , has been adopted for the stress increment

$$\Delta\sigma_i = \left(\frac{1}{2}\mathbf{D}' + \frac{1}{2}\mathbf{D}_i'^{+\Delta\epsilon_i}\right) \Delta\epsilon_i, \quad (13)$$

where  $\mathbf{D}_i'^{+\Delta\epsilon_i}$  is function of  $\epsilon_i'^{+\Delta\epsilon_i} = \epsilon_i' + \Delta\epsilon_i$  and  $\sigma_i'^{+\Delta\epsilon_i} = \sigma_i' + \mathbf{D}_i'^{+\Delta\epsilon_i} \Delta\epsilon_i$ . The previous algorithm can be employed with subincrementation, but it is important to integrate the stresses starting from the last converged configuration.

A convergence criterion has to terminate the equilibrium iteration as soon as the desired accuracy is achieved, but not before, and it should give the analyst complete control on the level of accuracy of the solution. Essentially, four quantities can be monitored during the iteration in order to establish a criterion: displacements, residual forces, incremental strain energy and some measure of the stiffness in the direction of the incremental displacement. Criteria based only on displacements or residuals can be misled by slow convergence rates. Energy criteria have proven to perform well in most cases [40]. The criteria chosen for this work can be expressed as

$$\frac{(\Delta\mathbf{u}_i^T \mathbf{r}_{i+1})}{(\Delta\mathbf{u}_i^T \mathbf{r}_i)} \leq (\text{tolerance}), \quad (14)$$

where the tolerance is taken equal to  $10^{-5}$ .

## NUMERICAL RESULTS

### Deep beam analysis

A classical benchmark of nonlinear finite element programs for the analysis of reinforced concrete beams is based on the experimental work by Leonhardt and Walther [18]. In that work several deep beams were tested up to failure and the results have been extensively documented. The beam denoted in [18] as WT-3, has been modeled with the proposed element, and the numerical predictions and experimental results are compared in the following paragraphs.

The beam has width of 9.9 cm, span of 160 cm, and depth of 160 cm. It is simply supported and subjected to a uniform load along its top edge. The dimensions and reinforcement arrangement are shown in Fig. 5(a). The main longitudinal reinforcement consists of four layers of two bars each

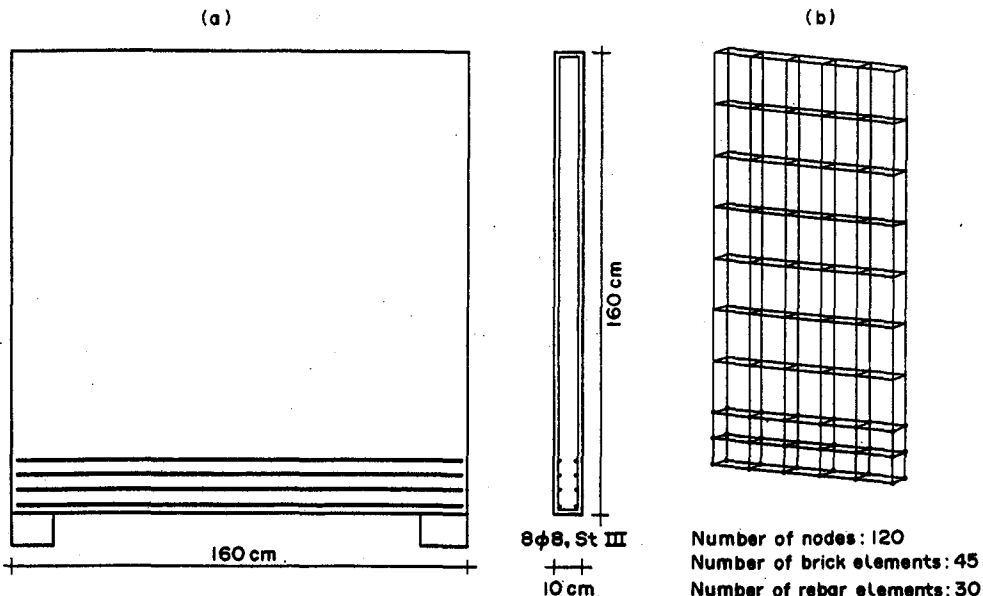


Fig. 5. Deep beam example: (a) dimensions and reinforcements; (b) deep beam (DB) mesh.

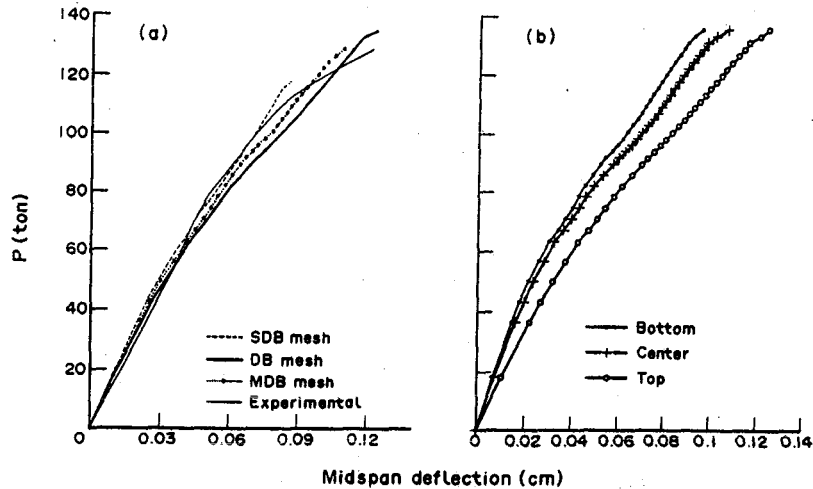


Fig. 6. Deep beam example: (a) analytical and experimental top midspan deflections; (b) analytical bottom, center and top midspan deflection.

anchored at the ends by means of hooks lying in a horizontal plane in order to prevent splitting. These bars have a diameter of 0.79 cm and a strength of 536.431 MPa. The web reinforcement is formed by a double net of orthogonal bars which have a diameter of 0.51 cm and a strength of 235.12 MPa. The concrete uniaxial compressive strength, modulus of rupture and initial Young's modulus are 29.649, 4.806 and  $31.7 \times 10^3$  MPa, respectively. The strain associated with the maximum uniaxial compressive stress is 0.002.

The deep beam described above has been modeled with three increasingly finer meshes denoted as SDB, MDB, and DB. SDB has 48 nodes and 15 brick elements, MDB is obtained from SDB by increasing the discretization in the lower midspan area to a total of 62 nodes and 21 brick elements, and finally DB, with 120 nodes and 45 bricks, as shown in Fig. 5(b), is the finer mesh.

Analytical and experimental midspan load-deflection curves are compared for the three meshes in Fig. 6a where relatively good agreement is observed. The failure load and deflection of the finer mesh are respectively 5% and 2% higher than the experimental ones. As expected, a stiffer response is obtained with the coarser mesh. In Fig. 6(b), the predicted deflections of the midspan at the bottom, center and top of the beam are plotted with the corresponding load for the DB mesh. The relative displacements of the three points show the nonlinearities which take place through the depth of the beam. The configuration at failure are shown in Fig. 7 for the DB mesh. In SDB and MDB the shear deformations in the support area are smaller than in DB. This is due in part to the shear locking effect of the linear isoparametric element, which is amplified by a course mesh.

Finally in Fig. 8 the progression of the damage pattern is illustrated. The disks represent cracks, while the spikes correspond to 'crashing' of concrete.

The material is said to crash when its stress state lies on the compressive softening branch of the constitutive model. The disks lie in the crack plane, and the segments plotted normally to the disks, represents the direction of the maximum tensile principal stress. Both symbols are located at the Gauss points where the failure conditions are met.

The distribution of the structural damage is reported at 37%, 68%, 84% and 100% of the failure load. At about 37% of the ultimate load the concrete in the support area starts entering the compression softening branch and tensile cracks occur at the bottom of the beam. The process gradually develops until instability is reached at a load of 135.1 ton due to crushing and cracking at the support areas. The previous analytical predictions are in good agreement

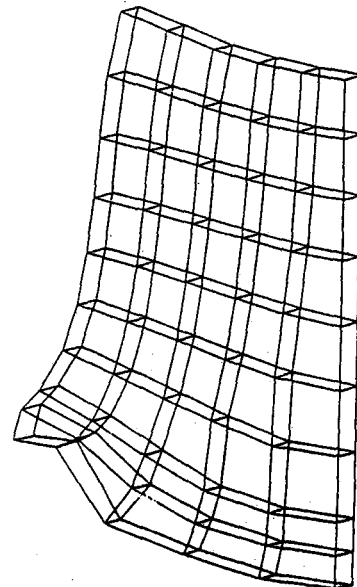


Fig. 7. Deep beam example: magnified deformed configuration at failure.

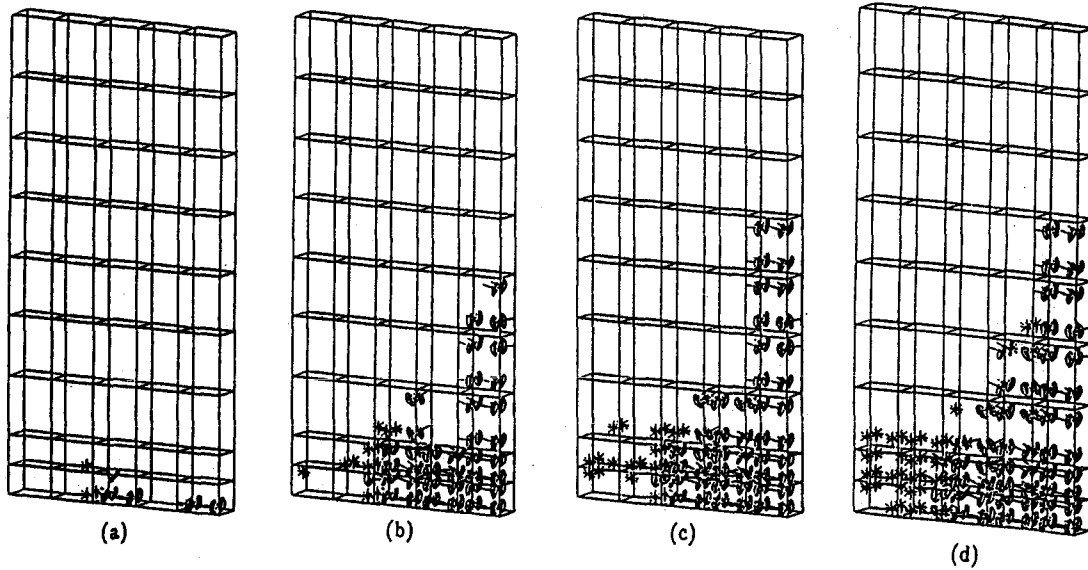


Fig. 8. Deep beam example: (a) damage pattern at  $P = 49.44$  ton; (b) damage pattern at  $P = 91.92$  ton; (c) damage pattern at  $P = 113.5$  ton; (d) damage pattern at  $P = 135.1$  ton.

with the experimental results obtained in [18] where failure load was reached at a load of 129.0 ton.

*Prestressed concrete reactor vessel analysis*

A prestressed concrete reactor vessel (PCRV) model, for which laboratory results are presented in [33], has also been studied with the proposed element in order to assess its behavior in a truly three-dimensional state of stress.

The PCRV model is fully described in [33]. A cylindrical concrete structure with a depth of 101.6 cm and diameter of 101.6 cm, with an end slab on the top with a thickness of 31.75 cm is connected at the bottom to a steel disk with thickness of 10.16 cm. The end slab contains six equally spaced cylindrical cavities.

The PCRV is presented by two post-tensioning systems. A linear prestressing system of 60 steel rods of 1.91 cm of diameter is used to develop vertical compressive stresses, and a circumferential prestressing system of 0.15 cm diameter wires located on the outside surface of the PCRV develops radial and circumferential compressive stresses. The concrete uniaxial compressive strength and initial Young's modulus are 39.44 and  $26.2 \times 10^3$  MPa, respectively. The strain associated with the peak uniaxial compressive stress is 0.00263, and the Poisson's modulus is 0.15. For the steel, the Young's modulus is  $206.85 \times 10^3$  MPa, the Poisson's modulus is 0.3, and the yield strength is 275.8, 965.3 and 1930 MPa for the base plate, the vertical tendons, and the circumferential wires, respectively. After the prestressing forces are applied, the PCRV is pressurized with increasing internal pressure up to failure.

Due to the symmetry of loading and geometry, only a 30° wedge of the PCRV has been modeled in the finite element analysis. The mesh and the bound-

ary conditions adopted in the model are shown in Fig. 9.

In the analysis the prestressing forces are applied before the internal pressure in an incremental fashion.

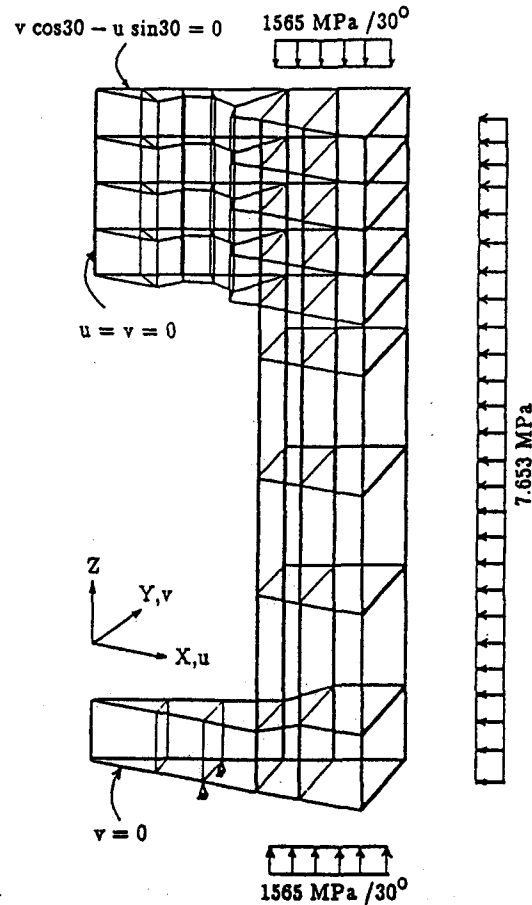


Fig. 9. PCRV example: finite element model.

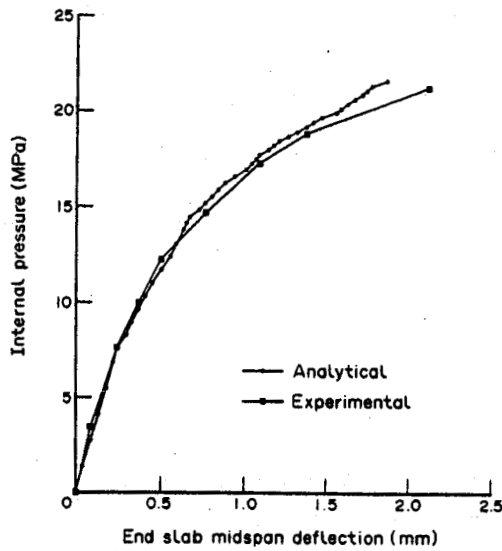


Fig. 10. PCRV example: analytical and experimental slab midspan deflections.

The pressure is then gradually applied to the vessel which reaches instability at 21.580 MPa. The predicted ultimate pressure favorably compares with the experimental failure pressure of 21.240 MPa. Figure 10 shows good agreement over the entire loading range between the analytical and experimental deflections at the midspan of the end slab. Finally the deformed configurations corresponding to the prestressing forces only, and to 44%, 86%, and 100% of the ultimate internal pressure are presented in Fig. 11. At 50% of the failure pressure, cracking initiated at the center of the outside surface of the end

slab, and crashing originated in regions around the penetration. The deformed configuration at failure suggests that the concentrated damage to the concrete surrounding the penetration strongly influenced the nonlinear response of the PCRV.

#### CONCLUSIONS

The field of finite element analysis of reinforced concrete structures, is gradually reaching maturity, after more than 20 years of research endeavor, and the emphasis is now on the reliability and computational efficiency of the more sophisticated models being proposed for this type of analysis. This work presented our effort in this context, in particular the (1) extension and recalibration of an accurate and numerically efficient bounding surface model for the behavior of concrete in cyclic compression, (2) the development of a complete constitutive relation for reinforced concrete by combining the bounding surface model with numerical procedures for the modeling of crack propagation, tension stiffening and steel reinforcement interaction effect, (3) the implementation of the constitutive model in a three-dimensional isoparametric eight-node element, and finally, (4) the verification of the accuracy of the current element by detailed analysis of a deep beam and a prestressed concrete reactor vessel which favorably compared with the experimental results. Recommendations for future work include the extension of dynamic analysis, and to the nonlinear analysis of reinforced concrete shells, as outlined in the following.

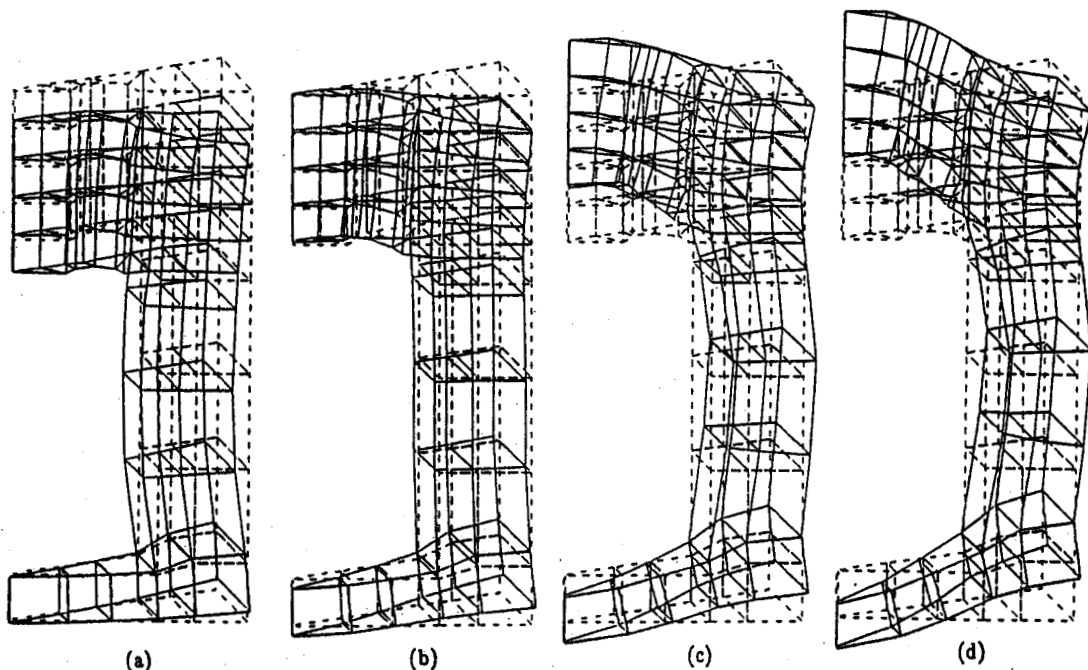


Fig. 11. PCRV example: magnified deformed configurations. (a) Prestressing forces only; (b) 44% of failure pressure; (c) 86% of failure pressure; (d) failure pressure.

Even though the adopted constitutive model for the behavior of concrete in compression allows (within the limitations previously presented) for the prediction of the rate independent cyclic response of the material, no attempt has been made to provide all the necessary additional features, such as bar slip and bond deterioration or the opening and closure of multiple cracks required for dynamic analysis. Alternative methods have been suggested [34-37] to cope with these problems and their incorporation in the proposed element would greatly enhance its range of applicability with a relatively modest additional effort.

Another important potential application of this work lies in the field of nonlinear reinforced concrete shell analysis. The usual 'layered' shell elements, composed of layers assumed to be in plane state of stress, have several disadvantages [38] which suggest the use of a computationally efficient fully three-dimensional element. The proposed element is a good candidate for this class of problems and benchmark tests to check its accuracy in this context are desirable and should be undertaken.

*Acknowledgements*—We gratefully acknowledge the National Science Foundation, for providing the financial support under the Research Initiation Grant during the early stage of the research, the Sloan Foundation, and the University of Rome for providing partial funding in the last year of the research.

#### REFERENCES

1. E. S. Chen and O. Buyukozturk, Constitutive model for concrete in cyclic compression. *J. Engng Mech., ASCE* 111, 797-814 (1985).
2. R. Ameer-Moussa, Constitutive modeling of concrete in finite element analysis. Thesis submitted in partial fulfillment for the degree of Master of Science, Department of Civil Engineering, MIT, Cambridge, MA (1987).
3. O. Buyukozturk and S. S. Shareef, Constitutive modeling of concrete in finite element analysis. *Comput. Struct.* 21, 581-610 (1984).
4. W. F. Chen and E. Yamaguchi, On constitutive modeling of concrete materials, *Proceedings of the Seminar sponsored by the J.S.P.S and the N.S.F.*, Tokyo, May 1985, (Edited by C. Meyer and H. Okamura), pp. 48-71, ASCE (1986).
5. D. J. Han and W. F. Chen, Constitutive modeling in analysis of concrete structures. *J. Engng Mech.* 113, 577-593 (1987).
6. K. A. Soon, Behavior of pressure confined concrete in monotonic and cyclic loadings. Thesis submitted in partial fulfillment for the degree of Doctor of Philosophy, Department of Civil Engineering, MIT, Cambridge, MA (1987).
7. J. G. M. Van Mier, Strain-softening of concrete under multiaxial loading conditions. Ph.D. thesis, Technische Hogeschool Eindhoven (1984).
8. M. D. Kotsovos and J. B. Newman, A mathematical description of the deformational behaviour of concrete under complex loading. *Magazine of Concrete Research* 31, 77-90 (1979).
9. M. D. Kotsovos and J. B. Newman, Mathematical description of deformational behavior of concrete under generalized stress beyond ultimate strength. *ACI JI* 77, 340-346 (1980).
10. H. Kupfer, H. K. Hilsdorf and H. Rusch, Behavior of concrete under biaxial stresses. *ACI JI* 66, 656-666 (1969).
11. O. Buyukozturk and J. Zisman, Behavior of concrete in biaxial cyclic stress. *Proceedings of the BOSS 82 Conference on the Behavior of Offshore Structures*, Vol. 2, No. S13, pp. 235-253 (1982).
12. I. D. Karsan and J. O. Jirsa, Behavior of concrete under compressive loadings. *J. Struct. Div., ASCE* 95, 2543-2563 (1969).
13. T. C. Y. Liu, A. H. Nilson and F. O. Slate, Stress-strain response and fracture of concrete in uniaxial and biaxial compression. *ACI JI* 69, 291-295 (1972).
14. G. Schickert and H. Winkler, Results of tests concerning strength and strain of concrete subjected to multiaxial compressive stresses. *Deutscher Ausschuss für Stahlbeton*, Heft 277. Wilhelm Ernst & Sohn, Berlin (1977).
15. M. E. Tasuji, A. H. Nilson and F. O. Slate, Biaxial stress-strain relationships for concrete. *Magazine of Concrete Research* 31, 217-224 (1979).
16. O. Buyukozturk and T. M. Tseng, Concrete in biaxial cyclic compression. *J. Struct. Engng* 110, 461-476 (1984).
17. D. Ngo and A. C. Scordelis, Finite element analysis of reinforced concrete beams. *Am. Concrete Inst. JI* 64, 152-163 (1967).
18. F. Leonhardt and R. Walther, *Wadertige Trager*. Deutscher Ausschuss für Stahlbeton, Heft 178. Berlin (1966).
19. Y. R. Rashid, Analysis of prestressed concrete pressure vessels. *Nucl. Engng Design* 7, 334-344 (1968).
20. Z. P. Bazant and L. Cedolin, Finite element modeling of crack band propagation. *J. Struct. Engng, ASCE* 109, 69-92 (1983).
21. Z. P. Bazant and B. H. Oh, Crack band theory for fracture of concrete. *Material and Structures, RILEM* 16, 155-177 (1983).
22. J. G. Rots, P. Nauta, G. M. A. Kusters and J. Blaauwendraad, Smeared crack approach and fracture localization in concrete. *Heron* 30, (1) (1985).
23. J. Blaauwendraad, Realizations and restrictions, application of numerical models to concrete structures. *Proceedings of the Seminar on Finite Element Analysis of Reinforced Concrete Structures*, Tokyo, May 21-24 (1985).
24. R. I. Gilbert and R. F. Warner, Nonlinear analysis of reinforced concrete slabs with tension stiffening. UNI-CIV Report No. R-167, University of New South Wales, Kensington, N.S.W. (1977).
25. C. S. Lin and A. Scordelis, Nonlinear analysis of RC shells of general form. *J. Struct. Div., ASCE* 101, 523-538 (1975).
26. A. Scanlon, Time dependent deflections of reinforced concrete slabs. Thesis submitted in partial fulfillment for the degree of Doctor of Philosophy, University of Alberta, Edmonton, Alberta (1971).
27. F. Damjanic, Reinforced concrete failure prediction under both static and transient conditions. Ph.D. thesis, C/Ph/71/83, University of Wales, Swansea (1983).
28. E. Hinton, H. H. Abdel Rahman and O. C. Zienkiewicz, Computational strategies for reinforced concrete slab systems. *IASBE Colloquium on Advanced Mechanics of RC*, Final report, pp. 303-313, Delft (1981).
29. K. H. Gerstle, Material modeling of reinforced concrete. Introductory report, *IASBE Colloquium on Advanced Mechanics of RC*, Final report, Delft, Vol. 33, pp. 41-63 (1981).
30. D. V. Phillips and O. C. Zienkiewicz, Finite element nonlinear analysis of concrete structures. *Proc. Inst. Civ. Engrs* 61, 59-88 (1976).

31. F. Damjanic and D. R. J. Owen. Practical considerations for modeling of post-cracking concrete behavior for finite element analysis of reinforced concrete structures. *Proc. of the International Conference on Computer-aided Analysis and Design of Concrete Structures*, pp. 693-706. Split, Sept (1984).
32. D. R. J. Owen and C. M. B. R. Gomes, An appraisal of numerical solution techniques for nonlinear problems. Paper M3/1, 6th SMiRT, Paris (1981).
33. J. Reins *et al.*, Shear strength of end slabs of prestressed concrete nuclear reactor vessels. Structural Research Series No. 429, University of Illinois (1976).
34. ASCE Task Committee on Finite Element Analysis of Reinforced Concrete Structures, State-of-the-Art Report on 'Finite element analysis of reinforced concrete'. ASCE Special Publications (1982).
35. *Proceedings of International Conference on Computer-aided Analysis and Design of Concrete Structures*, Parts 1 and 2, Split, September 17-21 (1984).
36. *Proceedings of the Seminar on Finite Element Analysis of Reinforced Concrete Structures*, Tokyo, May 21-24 (1985).
37. *Report of IABSE Colloquium on Computational Mechanics of Concrete Structures—Advances and Applications*, Delft (1987).
38. M. Cervera, E. Hinton and O. Hassan, Nonlinear analysis of reinforced concrete plate and shell structures using 20-noded isoparametric brick elements. *Comput. Struct.* 25, 845-869 (1987).
39. J. H. Argyris, Recent advances in matrix methods of structural analysis. In *Progress in Aeronautical Science*, Vol. 4, Pergamon Press, New York (1964).
40. K. J. Bathe and A. P. Cimento, Some practical procedures for the solution of nonlinear finite element equations. *Comp. Meth. Appl. Mech. Engng* 22, 59-85 (1980).
41. Z. P. Bazant and L. Cedolin, Fracture mechanics of reinforced concrete. Structural Engineering Report No. 79-9/640m, Northwestern University, Evanston, IL (1979).
42. Z. P. Bazant and S. S. Kim, Plastic fracturing theory of concrete. *J. Engng Mech. Div., ASCE* 105, Proc. paper 14653, 407-428 (1979).
43. Z. P. Bazant and C. L. Shieh, Hysteretic fracturing endochronic theory for concrete. *J. Engng Mech. Div., ASCE* 106, Proc. paper 15781, 929-950 (1980).
44. S. H. Crandall, *Engineering Analysis—A Survey of Numerical Procedures*. McGraw-Hill (1956).
45. M. A. Crisfield, Accelerated solution techniques and concrete cracking. *Proc. FENOMECH 2, Comp. Meth. Appl. Mech. Engng* 33, 585-607 (1982).
46. M. N. Fardis, B. Alibe and J. L. Tassoulas, Monotonic and cyclic constitutive law for concrete. *J. Engng Mech., ASCE* 109, Proc. paper 17871, 516-536 (1983).
47. M. D. Kotsovos, Concrete—a brittle fracturing material. *Material and Structures, RILEM* (1984).
48. B. M. Irons and S. Ahmad, *Techniques of Finite Elements*. Ellis Horwood, Chichester (1980).
49. A. H. Nilson, Nonlinear analysis of reinforced concrete by the finite element analysis. *Am. Concrete Inst. JI* 65, 757-766 (1968).

#### APPENDIX: MATERIAL PARAMETERS OF THE BOUNDING SURFACE MODEL

##### Pre-failure parameters

Elastic constants. Initial Poisson's ratio,  $\nu = 0.17$ , initial Young's modulus modulus,  $E = 57,000(\epsilon_0/\sqrt{f'_c})$ , resulting in an initial shear modulus

$$G = 24,360 \frac{\epsilon_0}{\sqrt{f'_c}}$$

Tangent bulk modulus. For hydrostatic loading

$$K_t = \frac{28,790}{1 + 0.358I_1^{1.5}} \frac{\epsilon_0}{\sqrt{f'_c}}$$

For hydroaxis unloading

$$K_t = 28,790 \frac{\epsilon_0}{\sqrt{f'_c}}$$

Plastic shear modulus. For deviatoric loading

$$H^p = \frac{R}{F_1(I_1, \theta)} \frac{2.4(1-D)^{0.65D^2}}{(1 + 0.7K_{\max}^2)A_L}$$

$$A_L = 1.02 - 0.81K_R/K_{\max}, \quad K < K_{\max}$$

$$A_L = 1, \quad K = K_{\max}$$

$K_R$  is the value of  $K$  at the beginning of recent loading. For deviatoric unloading

$$H^p = \frac{R}{F_1(I_1, \theta)} \frac{2.4}{(1 + 0.7K_{\max}^2)A_u}$$

$$A_u = 0, \quad K < 0.2K_{\max}$$

$$A_u = \frac{K_u - 0.2K_{\max}}{0.8K_{\max}}, \quad K \geq 0.2K_{\max}$$

$K_u$  is the value of  $K$  at the beginning of recent unloading. Shear compaction-dilatancy factor.

$$\beta_1 = 1.1 \exp[-30(K_{\max} - 0.6)^2], \quad K = K_{\max}$$

$$\beta_1 = 0, \quad K < K_{\max}$$

$$\beta_2 = -1.97\lambda \exp(-2\lambda^2)$$

$$\lambda = D - 0.2K_{\max}^2$$

$$\beta = \beta_1 + \beta_2$$

##### Post-failure parameters

Shear modulus,  $G = 50$ , tangent bulk modulus,

$$K_t = 28,790(\epsilon_0/\sqrt{f'_c})$$

dilatancy factor,  $\beta = -1.97\lambda \exp(-2\lambda^2)$  and

$$\lambda = 1 - 0.2K_{\max}^2$$

Plastic shear modulus

$$H^p = -0.15 \exp[-0.025(K_{\max} - 1)^2] F_2(I_{1,\max})$$

where

$$F_2(I_{1,\max}) = \frac{0.14}{(I_{1,\max})^2 - 0.86}, \quad I_{1,\max} \leq 2.54$$

$$F_2(I_{1,\max}) = 0.025, \quad I_{1,\max} > 2.54$$